Materials Transactions, Vol. 65, No. 5 (2024) pp. 541 to 551
©2024 Japan Foundry Engineering Society

Observation and Numerical Prediction of Concentration Distribution at Cast Coating Interface of Solid Pt, Ir, Re Using Liquid Ni-Based Alloys*1

Machiko Ode*2, Hisao Esaka, Akira Ishida, Susumu Takamori and Hideyuki Murakami

National Institute for Materials Science, Tsukuba 305-0047, Japan

The applicability of a cast-coating process for improving the oxidation resistance of cast Ni-based superalloys was evaluated. Specifically, metallic plates of Pr, Ir, and Re expected to improve oxidation resistance when they are enriched on the cast alloys were placed in a mold and cast coating using Ni-10at%Al alloy was performed in order to investigate the formation of the Pt, Ir, or Re-enriched layer on the casting surface. Then the microstructure of the Ni-based alloy/specimen interface was observed. To analyze the concentration profile in the interdiffusion region, solidification and diffusion simulations were performed. It was found that Pt easily dissolves into the molten Ni-based alloy, and Re cannot expected to modify cast metal surfaces due to its low solubility into the Ni-10at%Al alloy. On the other hand, Ir forms smooth interdiffusion layer, and numerical calculations predicted that Ir can maintain the modification ability even in a process time of 1 hour, which is equivalent to the casting time of Ni-based turbine blades. [doi:10.2320/matertrans.F-M2024805]

(Received December 6, 2023; Accepted February 2, 2024; Published March 8, 2024)

Keywords: *cast-coating, Ni-base superalloy, solid/liquid interface, solidification simulation*

1. Introduction

Platinum group metals and rare metals generally have a high melting point and many have excellent mechanical properties at high temperatures, oxidation resistance, corrosion resistance and catalytic performance.[1)] However, since they are very expensive, a method is required, which can unevenly distribute them on the surface of the component in a way that is suitable for each application. For example, in the case of catalytic applications, in order to cover sufficient surface area of the catalyst material, it is attached to the surface of the carrier as fine particles achieving both material savings and catalytic performance. Similarly, when using the oxidation and corrosion resistance properties of platinum group metals, high cost performance can be achieved by forming a dense thin film covering the surface of the base material.

The plating method is the industrially cheapest thin-film deposition process due to its inexpensive equipment, which produces little waste of raw materials. However, some rare metals such as W and Re are difficult to plate. On the other hand, physical vapor deposition methods such as sputtering and PVD are adaptable to various materials but expensive processes in terms of material yield. In principle, the inner wall surface of hollow components cannot be modified. Therefore, there is a need to develop a process that is inexpensive, simple and can uniformly modify all surfaces of components. Ni-based superalloy turbine blades have a two-layer coating on the outside for oxidation resistance and heat shielding, and a cooling circuit on the inside for air-cooling the turbine blades. Such improvements in internal and external system allow Ni-based alloy blades to be used at operating temperatures above their melting point. However, as a result of the higher operating temperatures, oxidation of the uncoated inner blade wall has become a problem.

The cast-in insert method is one of the casting techniques employed to obtain surface-modified metallic materials. In this method, a component with a higher melting point than the molten metal temperature is placed in the mold in advance. The casting and the component are added during casting to combine different materials while taking advantage of the moldability of casting.[2,3)] In another method, the coated casting process,[4)] the surface of the casting material is modified by first coating the mold surface with a slurry of cemented carbide powder such as titanium or WC, and then casting Mg, Al alloy, steel or cast iron into it.[5–7)] This is also referred to as a cast coating. In both cases, good control of the reaction between the molten metal and the solid metal in the casting process is necessary to achieve the required properties. The aim of this study was to evaluate whether it is possible to modify the surface of Ni-based alloy castings by applying the above metallic elements to the surfaces of molds and cores for using expensive elements more efficiently. Three elements were selected: the two from platinum group metals, Pt and Ir, and a rare metal with a high melting point, Re. The platinum group metal Pt is already in practical use as an oxidation-resistant bond coating for Ni-based superalloys. The other metals Re and Ir have particularly high melting points, among the elements under research and development. First, in order to gain a basic understanding of the process, small pieces of Pt, Ir and Re metal were cast-coated on a Ni alloy, and the interface was observed. Then, to gain knowledge about the interaction between the solid metal and the molten metal, the temperature change of the metallic pieces during casting was predicted by solidification heat transfer calculations. The theoretical calculations of the interfacial diffusion layer were carried out using the obtained temperature changes as input conditions for thermodynamic calculation software. Based on the results, it is discussed whether surface modification with Pt, Ir and Re as the main elements can be obtained by the casting method. For clarity, casting for the purpose of surface modification will henceforth be referred to as cast-coating in this paper.

*1This Paper was Originally Published in Japanese in J. JFS **94** (2022) 673–683. Some spelling errors were modified.
*2Corresponding author, E-mail: ODE.Machiko@nims.go.jp

2. Methods

2.1 Casting experiment

About 2 kg of Ni-10at%Al alloy was melted in a vacuum induction melting furnace and poured into a mold fixed with small pieces of pure Pt, Ir and Re (approximately 20 mm long, 10 mm wide and 1 mm thick). A schematic diagram of the experimental apparatus and a detailed drawing of the mold are shown in Fig. 1. The heat flow was controlled in one direction by using a rectangular mold, which had 18 mm-thick SUS on one side and ceramic insulation on other sides. There are two methods for fixing the Pt, Ir, and Re samples. In one method, they are directly affixed to the SUS plate surface using an inorganic adhesive. In the other method, they are fixed to a cylindrical quartz glass stand with slits using an inorganic adhesive. These assemblies are then positioned at 20 mm and 40 mm from the SUS plate on the bottom of the mold. The contact time of the sample with the molten metal changes according to the distance between the sample and the SUS plate. Therefore, the dependence of the interfacial reaction of the sample/Ni-based alloy on the molten metal contact time can be verified.

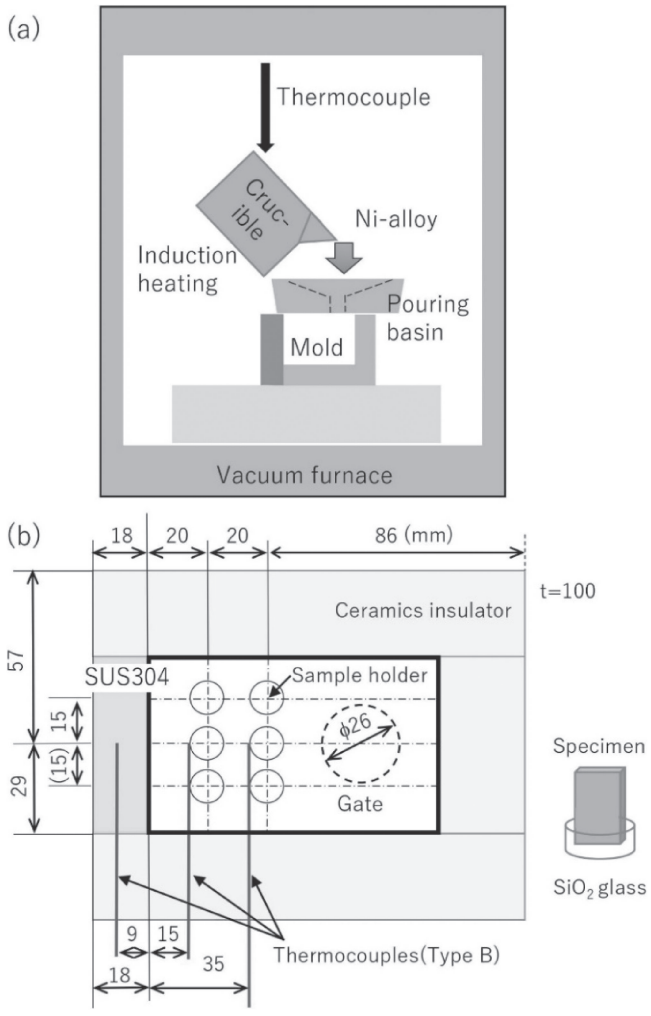

Fig. 1 Experimental apparatus. (a) Schematic of vacuum-induction furnace. (b) Top view of the mold. Approximately 2 kg of Ni-10at%Al alloy was melted in the vacuum-induction furnace and cast into the mold in which pure Pt, It, and Re specimens are fixed.

Temperature changes in the mold were measured using three B type thermocouples. The height of the thermocouples in the mold was approximately 20 mm from the bottom of the mold. Their positions in the direction of heat flow were 15 mm and 35 mm from the SUS plate surface and SUS plate center, respectively. Temperatures were obtained using a data logger (GRAPHTEC GL200A) with a time interval set to 0.1 second. Casting experiments were carried out once each at different casting temperatures of approximately 1650°C, 1600°C and 1500°C. In this experiment, as Pt samples were found to dissolve easily, the Pt sample was only placed on the SUS plate surface in the case of 1600°C casting temperature. A sample was cut from the ingot and mirror polished. The microstructure and concentration distribution near the interface between the sample and the Ni-based alloy were observed using SEM-EDX (Hitachi High-Tech S4700).

2.2 Simulations

Two different type of computer simulations were carried out. The first was for estimating the temperature of the sample during casting by comparing temperature measurements from casting experiments with solidification heat transfer calculations. The second was for predicting the concentration near the interface between the sample and the Ni-based alloy using the temperature obtained from the heat transfer calculations as input value. For validation of the latter, the concentration distribution calculated by the simulation were compared with experimental observations. The ability to apply cast-coating to long solidification processes such as turbine blade casting was investigated based on the verified prediction method.

Figure 2 shows the schematic illustration of calculation system and temperature distribution. Assuming that the adiabatic conditions are satisfied except for the SUS plate, the heat flow is assumed to be in one direction. The enthalpy method was used in the heat transfer calculations. The enthalpy method is outlined below.

The enthalpy at temperature T in the solid-liquid coexistence temperature range is expressed as follows.

$$H(T) = H_0 + \int_{T_0}^{T} C_p dT + (1 - f_s)L \qquad (1)$$

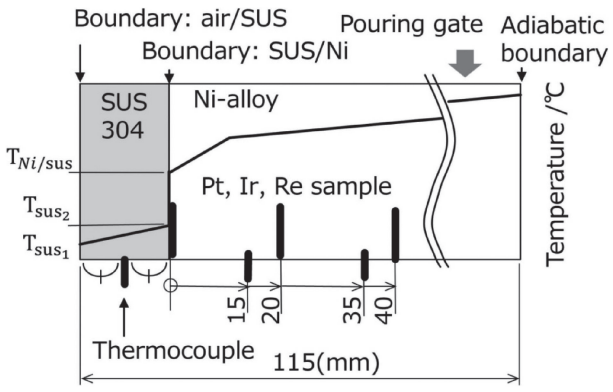

Fig. 2 Schematic illustration of calculation system. The heat flow can be regarded as unidirectional, so that the temperature distribution could be represented by a one-dimensional calculation.

Where H_0 is the enthalpy of the standard state, C_p is the specific heat, L is the latent heat of solidification and f_s is the solid fraction. Partial differentiation of eq. (1) with temperature results in the specific heat in the solid-liquid coexistence temperature range taking into account the latent heat of solidification, as shown in eq. (2).

$$\frac{\partial H}{\partial T} = C_p - \frac{\partial f_s}{\partial T} L \tag{2}$$

By defining the effective specific heat $C_{P_{eff}}$ as

$$C_{P_{eff}} = \begin{cases} C_p \\ C_p - \dfrac{\partial f_s}{\partial T} L \quad (T_S < T < T_L) \end{cases} \tag{3}$$

The relationship between specific heat and enthalpy is as follows, regardless of whether it is a single-phase or solid-liquid coexisting state.

$$\frac{\partial H}{\partial T} = C_{P_{eff}} \tag{4}$$

where T_L is the liquidus temperature and T_S is the solidus temperature.

The governing equations are derived with a focus on numerical computations. First, we consider a small unit volume (computational grid) with a surface area ΔA and volume ΔV. Let J be the amount of heat (heat flux) flowing through the unit surface per unit time Δt, then relationship between J and the time variation of temperature can be derived from the energy conservation law and the continuity equation as

$$C_{P_{eff}} \frac{\Delta T}{\Delta t} = \frac{\Delta A}{\Delta V} J \tag{5}$$

Using $\Delta A/\Delta V = 1/\Delta x$ for one-dimension case, where Δx is the unit length, and substituting eq. (4) into eq. (5), the following equation is obtained.

$$\frac{\Delta H}{\Delta t} = \frac{J}{\Delta x} \tag{6}$$

The heat flux J was classified into four categories, including inside the ingot and three types of boundaries, as shown below.

i) Inside the ingot

The heat flux inside the SUS plate is assumed to follows Fourier's law.

$$J = \lambda \frac{\partial T}{\partial x} \tag{7}$$

where λ is the thermal conductivity of SUS.

ii) Because surfaces other than the SUS plate were thermally insulated,

$$J = 0 \tag{8}$$

iii) Assuming that the heat dissipation from the SUS plate surface follows Newton's law of cooling, the heat flux is,

$$J = h_{air}(T_{sus1} - T_{\text{furnace}}) \tag{9}$$

where h_{air}, the heat transfer coefficient is assumed constant in this study, T_{sus1} is the outer surface temperature of the SUS plate and T_{furnace} is the internal temperature of the furnace, which was set to 50°C based on actual measurements before casting.

iv) The heat transfer between the SUS plate and the Ni-based alloy is assumed to be the same as shown in eq. (9) above the solidification initiation temperature, T_c, because the Ni-based alloy is a fluid while it is in the liquid phase. On the other hand, after the start of solidification, a contact resistance, R^{-1}, exists between the SUS plate and the solidified layer, which can be shown as follows.

$$\begin{aligned} J &= h_{liq}(T_{sus2} - T_{Ni/sus}) \quad T_{Ni/sus} \geq T_c \\ J &= R^{-1}(T_{sus2} - T_{Ni/sus}) \quad T_{Ni/sus} < T_c \end{aligned} \tag{10}$$

$1/R = \kappa\lambda/\Delta x$, where κ is the contact conductance, the second line of eq. (10) is equivalent to Fourier's equation (7).

The values of h_{air}, h_{liq}, R^{-1} and T_c in each equation were determined by simulation and measured temperatures and are regarded as constants. The heat transfer coefficients are not constants and may vary considerably with temperature and time. However, the aim of this calculation is to estimate the sample temperature, not to obtain detailed values for the transfer coefficients. The transfer coefficients are assumed to be constants, because if the coefficients are assumed as functions of temperature and time, an infinite number of plausible combinations will be found. The heat transfer at the casting/mold interface decreases rapidly once solidification has started due to solidification shrinkage. Therefore, the number of parameters required for the calculation was reduced by setting $R^{-1} = \alpha \cdot h_{liq}$, $(\alpha = 0.1)$ to simplify the calculation for thermal resistance. If α is set to different values less than 1, the corresponding changes in h_{liq} have little effect on the desired computational prediction results.

In the numerical calculations, the heat flux is first obtained from the temperature distribution from eqs. (7)–(10) and the time variation of enthalpy from eq. (5). The temperature change is then determined from the temperature-enthalpy relationship in eq. (1). The temperature-enthalpy relationship was obtained from the Ni-10at%Al alloy equilibrium solidification calculation using CompuTherm's thermodynamic database PanNi2020a and the phase diagram calculation software PANDAT. The database is available for any binary combination of the five elements Ni, Al, Pt, Ir and Re in the entire composition range. For ternary systems, there are no compositional restrictions for the major phases in the Ni-Al-Pt and Ni-Al-Re systems and for the fcc phase and its equilibrium phase in the Ni-Al-Ir system.[8,9] From the calculation results, the temperature-enthalpy relationship can be approximated by eq. (11). The thermodynamic properties used in the calculation are given in Table 1. The enthalpy-

Table 1 Thermodynamic properties of Ni-10at%Al alloy used in simulations.

Property	
Heat capacity in liquid, c_l (J/(m^3°C))	6.26×10^6
Heat capacity in solid, c_s (J/(m^3°C))	5.5×10^6
Liquidus temperature, T_l (°C)	1445.4
Solidus temperature, T_s (°C)	1443.5
Enthalpy at liquidus, H_{T_l} (J/m^3)	7.23×10^9
Enthalpy at solidus, H_{T_s} (J/m^3)	4.36×10^9
Heat conductivity, λ (W/(m°C))	79.6

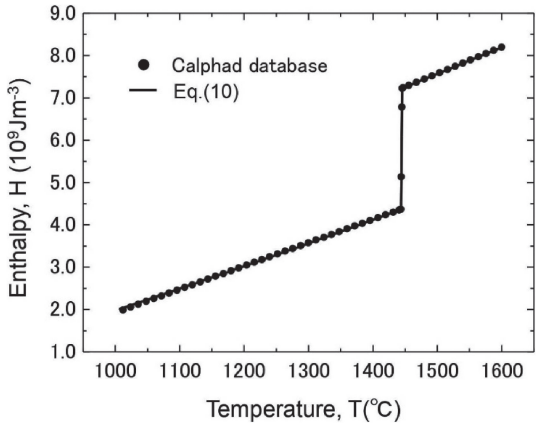

Fig. 3 Enthalpy change depending on temperature for Ni-10at%Al alloy obtained by equilibrium solidification simulation using PANDAT and PanNickel thermodynamic database.

temperature relationship thus obtained is shown in Fig. 3. The values in Table 1 were selected giving priority to the reproducibility around the solid-liquid coexistence temperature. Therefore, the maximum error is observed in the temperature range away from the solid-liquid coexistence temperature, but the value is within about 2.5% even around 1000°C, where the error is the largest. The thermal conductivity of the alloys was obtained by linearly combining the data for pure Ni and pure Al from the Metals Data Book[10] by composition ratio.

$$\begin{aligned} H(T) &= H_{T_l} + c_l(T - T_l) && : T > T_l \\ H(T) &= H_{T_s} + \frac{\partial H}{\partial T}(T - T_s) && : T_s \le T \le T_l \\ H(T) &= H_{T_s} + c_s(T - T_s) && : T < T_s \end{aligned} \tag{11}$$

There are three parameters in the calculation: h_{air}, h_{liq} and T_c. These parameters were determined using the length of the liquidus temperature holding time of the thermocouple in the mold, which was obtained from actual measurements, as an indicator.

The governing equations were solved numerically in Python.

The second concentration field prediction was carried out using the Pandat diffusion module and the diffusion mobility database for Ni-based alloys (PanNi2020_MB). In the database, only the fcc phases of the Al-Ni, Al-Pt, Ni-Ir, Ni-Pt and Ni-Re systems relevant to this study were assessed. As the alloys used in this study have a high concentration of Ni-90at%, the calculated concentration profiles of the Ir and Pt samples and Ni can be used for discussion. The hcp phase has not been assessed, but reaction diffusion is expected to occur between the Re sample and the Ni-based alloys, where hcp phase is expected to precipitate phase diagram. This can be discussed qualitatively from the viewpoint of the equilibrium phase diagram as well as diffusion. The details of the specific input conditions are described in the section, temperature prediction by enthalpy method in results and discussion.

3. Results and Discussion

3.1 Temperature measurements and numerical predictions

3.1.1 Results of temperature measurements

Figure 4 shows the temperature variation during casting over a period of 600 s from the time of casting. In the temperature measurement at 1600°C, the thermocouple at 35 mm was disconnected at around 350 s. The temperature curve looks very smooth compared to the other two experiments because it is not influenced by the electrical noise from the power supply.

In the case of unidirectional solidification, the columnar dendrites grow in the direction opposite to the heat flow. During solidification, the growing tip is maintained at the liquidus temperature, so that the maximum temperature on the liquidus side decreases with time from the casting temperature and then remains at the liquidus temperature. Therefore, the temperature curve inside the casting forms a plateau that maintains the liquidus temperature for a certain time.[11] In all cases in this experiment, the thermocouple inside the casting formed a constant temperature plateau at about 1440°C. Furthermore, in all cases, the plateau temperature holding time at 15 mm from the SUS plate was shorter than that at 35 mm, indicating that solidification was proceeding unidirectionally from the SUS plate side. The holding time will be discussed in detail in the heat transfer calculation section. Figure 5 shows the calculated phase diagram of the Ni-Al binary system on the Ni-rich side. The liquidus temperature of the Ni-10at%Al alloy indicated by

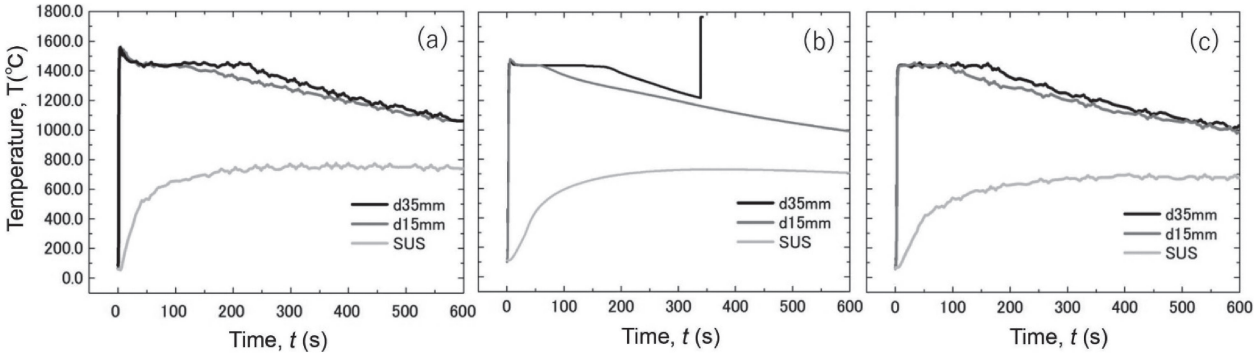

Fig. 4 Temperature change in the mold measured by thermocouples. The casting temperature is (a) 1650, (b) 1600 and (c) 1550°C, respectively. In all cases, the temperature curve obtained inside the casting shows a constant temperature plateau at about 1440°C and the holding time at 35 mm is longer than that at 15 mm. This result, "the farther the longer" suggests that the solidification progresses unidirectionally from the SUS plate side.

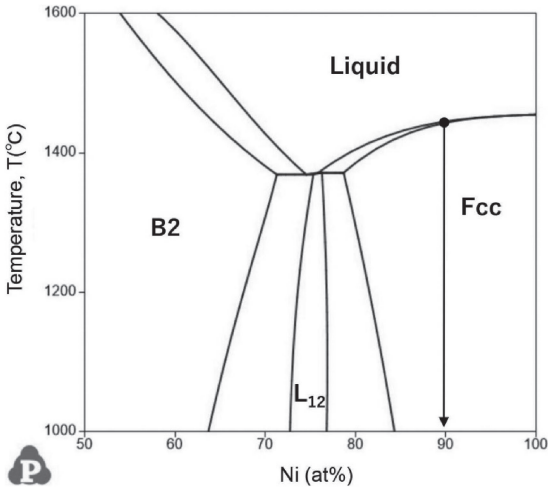

Fig. 5 Calculation phase diagram of Ni-Al binary system. The liquidus temperature of Ni-10at%Al is about 1455°C.

the arrow is about 1445°C, which is in good agreement with the experimentally measured plateau temperature.

The temperature of the thermocouple inside the SUS plate rises by absorbing heat from the molten metal. Under all casting conditions, the temperature quickly rises to around 600°C within about one minute after casting, and then continues to rise slowly before maintaining an almost constant temperature. This is because as the temperature of the SUS plate rises, the heat absorption of the SUS plate decreases while the amount of heat released into the furnace increases. The heat balance is practically achieved at a temperature, which remains almost constant until the generation of latent heat of solidification ceases. The temperature in the SUS plate at 600 s were 770°C, 707°C and 690°C, consistent with the casting temperatures of 1650°C, 1600°C and 1500°C, respectively.

3.1.2 Temperature prediction by enthalpy method

Figure 6 shows an example of the calculation results using the enthalpy method described in Section 2.2. It presents the variation of the temperature over time within the mold, as depicted in the schematic diagram in Fig. 2 (Fig. 6(a)). By plotting the relationship of temperature changes over time at both the thermocouple and sample positions, we can obtain temperature changes similar to those measured by the thermocouples (Fig. 6(b)). The temperature gradient in the solidifying casting across the solid liquid interface is higher on the solid side than on the liquid side due to the latent heat of solidification. After solidification is finished, the temperature distribution becomes smooth throughout the casting and the temperature difference within the casting becomes smaller. In other words, under the temperature condition shown in Fig. 2, the temperatures of the samples and thermocouples decrease maintaining a constant temperature difference even after the solidification process, as shown in Fig. 6(b). However, the temperatures of the two thermocouples shown in Fig. 4 relatively quickly converged after they becomes smaller than the plateau temperature at about 600 seconds. This may be due to the fact that the heat flow in the mold is not completely one-dimensional, but also flows towards the adiabatic wall and the top of the mold.

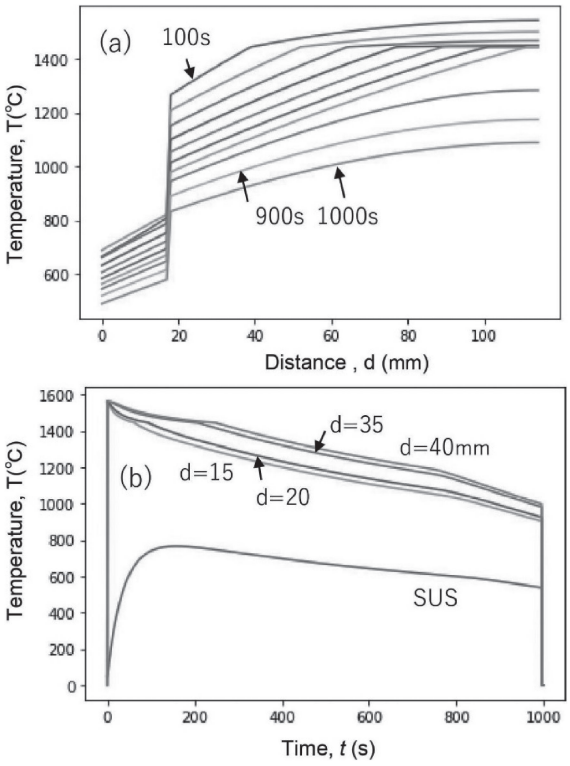

Fig. 6 Time change of the calculated temperature. (a) Temperature profile along heat flow. Each curve is drawn every 100 sec. Temperature gradient varies at the solid-liquid interface. (b) Temperature change by fixed point measurement. In the case of experiment (Fig. 4), the temperature difference between two points, d = 15 mm and d = 35 mm, shows maximum when the point, d = 35 mm, solidifies and then decreases. On the other hand, in the present simulation, the temperature difference hardly changes over a wide range.

However, the macroscopic shrinkage cavity, which were considered to be the final solidification region, were located near the gate. Thus, it can be concluded that unidirectional solidification was achieved at least up to the gate area. Specifically, unidirectional solidification is reliably achieved up to a sample temperature of 1440°C and it continues until approximately 1200°C, based on the results shown in Fig. 6(a). From the above, when estimating the sample temperature by numerical calculation, h_{air}, h_{liq} and T_c were determined to minimize the sum of the squares of the difference between the actual measurement of the plateau temperature holding time and its predicted time in the high temperature range, which have the greatest influence on diffusion.

For the prediction of the temperature plateau retention time, three parameters were explored in the realistic ranges as follows:

$$1000 < h_{air} < 50000 \quad \text{(increment: 500)}$$
$$1000 < h_{liq} < 50000 \quad \text{(increment: 1000)}$$
$$T_c = T_s - x$$
$$0 < x < 100 \quad \text{(increment: 10)}$$

Figure 7(a) shows the sum of squares of the difference between the experimentally measured and calculated temperature plateau holding time for a casting temperature of 1650°C. To visualize the error between the measured values and predicted values more clearly, the parameter x is fixed at

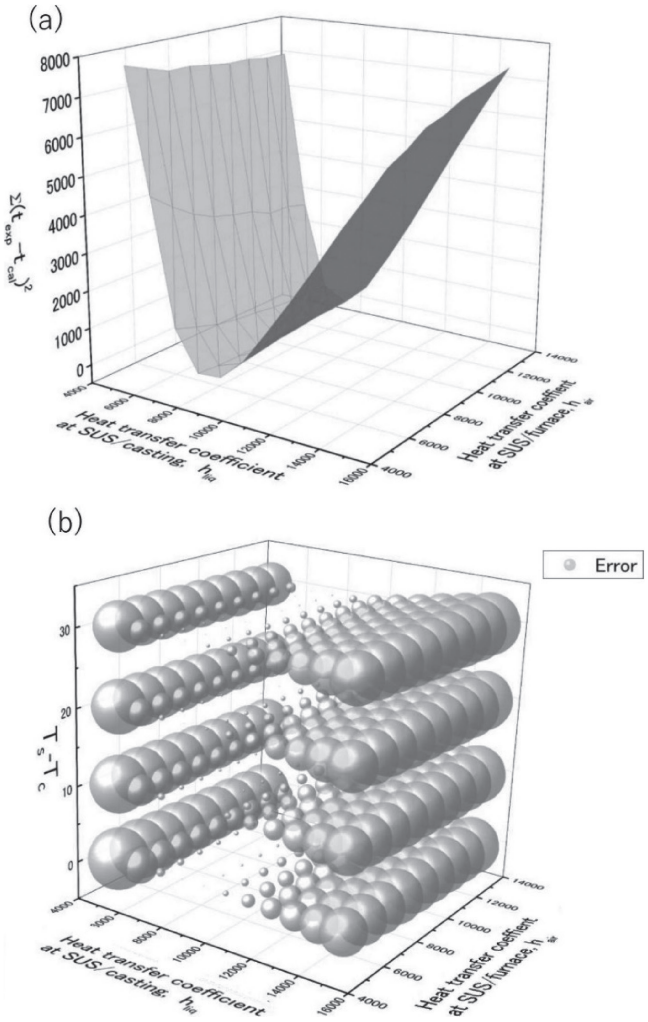

Fig. 7 Effect of calculation parameters on difference between measured and calculated holding time of temperature plateau. (a) The parameter T_c is fixed to T_s and X and Y axis represents heat transfer coefficients, h_{liq} and h_{air}, respectively. The effect of h_{liq} on the prediction error is much larger than that of h_{air}. (b) The parameter, T_c is treated as a valuable and assigned to the Z axis. The difference between calculated and measured time is expressed as the radius of the sphere at each parameter space. The parameter, h_{liq}, is dominant factor of the plateau time.

0°C, and the two horizontal axes are assigned to the heat transfer coefficients, h_{air} and h_{liq}. The figure shows that the heat transfer coefficient between the SUS plate interface and the casting, h_{liq}, is the dominant factor in the temperature prediction accuracy at $T_s - T_c = 0$°C. Figure 7(b) shows the sum of the squared time differences used for the vertical axis in Fig. 7(a) as the radius of the sphere, with $T_s - T_c$ on the vertical axis. The right side of the horizontal axis is h_{air} and the left side is h_{liq}. The smaller the radius of the sphere, the smaller the error is in predicting the plateau time, as shown in Fig. 7(a). The prediction accuracy is highly dependent on the change in h_{liq} and is less influenced by h_{air} and $T_s - T_c$. Considering the mold designed for one-dimensional heat flow and the calculation conditions, it is natural to expect that the heat is lost to the outside due to the heat transfer between the SUS/casting, and this is the dominant factor in the plateau holding time. The minimum prediction error is at $h_{air} = 6500\,\mathrm{W/m^2K}$, $h_{liq} = 8000\,\mathrm{W/m^2K}$, $T_s - T_c = 0$°C, with an error of $17\,\mathrm{s^2}$. Although h_{air} value is very large

Table 2 Comparison of plateau time interval (s) between experimental and simulation results.

	Distance from surface(mm)	Casting temperature (°C)		
		1650	1600	1500
Thermocouple	15	100	60	90
	35	230	170	165
Predicted by simulation	15	96	60	N/A
	20	128	85	109*
	35	231	170	N/A
	40	267	201	184*

* predicted by experiment

compared to the typical value of heat transfer coefficient in natural convection,[12] it is apparent from Fig. 7 that the dominant factor influencing prediction errors is h_{liq}. The contribution of h_{air} to these errors is negligible. Therefore, in order to appropriately optimize the value of h_{air}, no refinements to the model such as multidimensionalization the computational domain or parameterizing h as a function of time or temperature will be pursued. Table 2 summarizes the predicted values of the calculation and experimental results. Similar parametric optimization calculations were also performed at 1600°C. They showed that when h_{liq} as different ($9000\,\mathrm{W/m^2K}$) from the optimum parameter set at 1650°C, the plateau time was predicted with an error of less than $1\,\mathrm{s^2}$. On the other hand, when the molten metal temperature was 1500°C, the model could not predict the plateau retention time accurately. There are several reasons for this. Figure 4 shows that at casting temperatures of 1650 and 1600°C, the thermocouples in the molds recorded temperatures above the liquid phase line temperature immediately after casting. On the other hand, at 1500°C, the thermocouples show temperatures below the liquidus line temperature, suggesting that solidification has already started somewhere in the casting when the molten metal reaches the thermocouples. If solidification progresses unidirectionally from the SUS plate, the time for the thermocouple in the mold to hold the plateau should increase as the casting temperature increases. At the 35 mm position, the plateau holding time at 1500°C and 1600°C was 165 s and 170 s respectively. The higher the casting temperature, the longer the plateau retention time, and this is considered reasonable casting. However, at the 15 mm position, the plateau retention time was 90 s at 1500°C, which is 30 s longer than the casting temperature of 1600°C and is inconsistent with the time expected from the casting temperature. This result suggests that as the molten metal was not sufficiently superheated in the experiment at 1500°C, solidification and melting may have occurred inhomogeneously in time and space on the mold surface, resulting in the heat flow being more complicated and unidirectional than at 1650°C and 1600°C.

As a result, it is expected that the model assuming unidirectional solidification could not reproduce the plateau time accurately by parameter fitting. However, the liquid phase temperature holding time of the thermocouple was longer at the 35 mm position than at 15 mm. The results of cutting the castings showed that the shrinkage cavities, which were thought to be the final solidification area, were located just below the gate (as shown in Fig. 1), suggesting that

solidification was unidirectional overall even in the 1500°C sample. Therefore, plateau retention time at the sample position at a casting temperature of 1500°C was assumed to be proportional to the distance from the SUS plate, and the value estimated from the 1500°C thermocouple measurement was used.

The results show that the time, when the sample is in contact with the liquid phase, does not exceed 300 s, even for samples located far from the SUS plate. The plateau temperature time thus obtained from the calculations was employed in the concentration distribution simulation.

3.2 Microstructural observation and concentration distribution prediction

Figure 8 shows SEM image of the interface in the Ir sample placed at 40 mm from the surface of the SUS plate and the concentration distribution. The distance from the top of the sample on the opposite side of the SUS plate were 6 mm (1650°C) and 3 mm (1500°C), respectively. In the case of the Ir sample, the cast-coating layer with the Ni-based alloy was in a good diffusion bonding state and no difference was observed in the concentration distribution between the measurement positions (SUS side and opposite side, in the height direction from the bottom of mold). The thickness of the diffusion layer is indicated by the arrows: 25 μm at a molten temperature of 1650°C (Fig. 8(a)) and 20 μm at 1500°C (Fig. 8(b)). Here, the Al concentration in the Ir sample appears to vary with casting temperature is due to an analytical error and is not considered to be a significant difference. This is because the Al-Kα line in the EDS spectrum is too close to the Ir-Mζ line peak, so even if there is no Al in the Ir alloy sample, it can be misidentified as containing a small amount of Al.

Figure 9 shows the results of the Re sample placed at 40 mm and the molten temperature was 1500°C. The Re sample is characterized by the formation of a solute diffusion layer on the Re sample side only, even though no cracks were observed between the sample and the Ni-based alloy. As can be seen from the cross section, the Re sample has a sintered microstructure with a density of about 90%. The reason for the formation of the diffusion layer only on the Re side is not due to the effect of molten metal penetration into the sintered microstructure, as will be explained in the comparison with the diffusion simulation to be shown later. The Pt sample affixed directly to the SUS304 plate remained partially at both 1650°C and 1500°C, but the sample placed inside the casting was completely melted. The melting point of Pt is 1769°C, which is approximately 700°C lower than that of Ir (2443°C) and 1400°C lower than that of Re (3180°C). The equilibrium phase diagram also explains the ease of melting of Pt; Fig. 10 shows the Pt/Ni-10Alat% longitudinal sectional phase diagram. The liquid phase region extends well towards the low temperature side, and the liquidus temperatures of Ni-10at%Al and Ni-5Al-50at%Pt can be regarded as almost identical. In other words, the melting point of the Pt sample drops rapidly on the surface in contact with the Ni-10at%Al alloy due to interdiffusion, indicating that the Pt sample melts quickly even at around 1500°C.

The temperature change at the sample was estimated, and using this as an input condition, the PANDAT diffusion module and PanNi2020 mobility were used to calculate the concentration change near the sample and molten metal interface due to solute diffusion. The calculation system is one-dimensional and assumes a diffusion couple between one of the precious metal samples and the Ni-10at%Al alloy. As

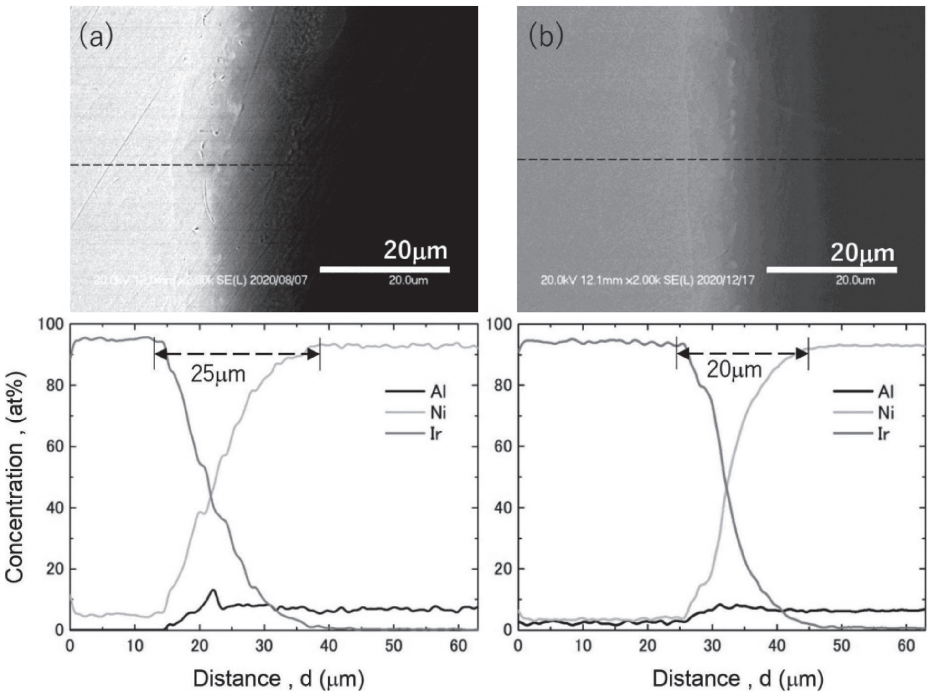

Fig. 8 Cross section in vicinity of Ir specimen/Ni-Al cast alloy interface and concentration profile obtained using SEM-EDS. The temperature of molten Ni-Al alloy is (a) 1650°C (b) 1500°C, respectively. In both cases, concentration profiles are smooth and there is no secondary phase in the diffusion zone.

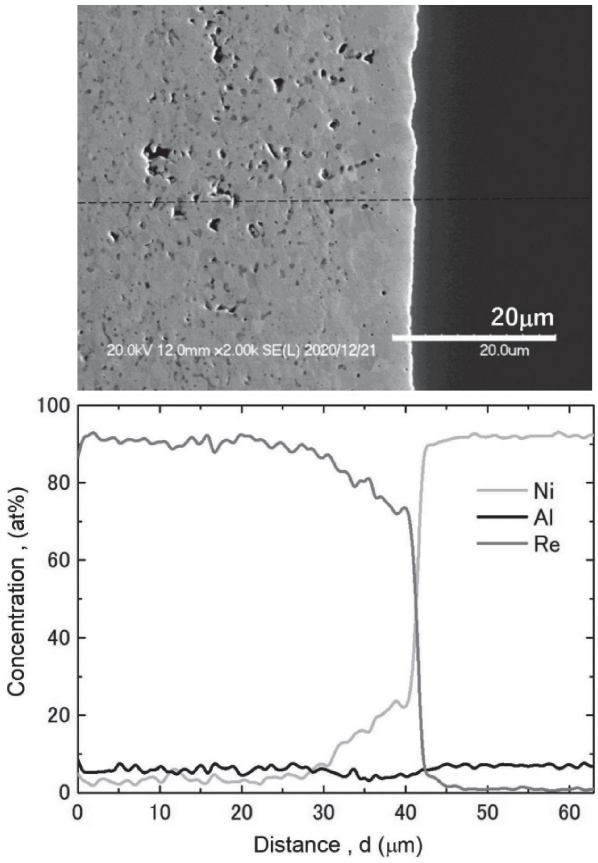

Fig. 9 Cross section in vicinity of Re specimen (d = 40 mm)/Ni-Al cast alloy interface and the concentration profile obtained using SEM-EDS. The casting temperature of Ni-Al alloy is 1500°C. Solute partitioning occurs at the interface.

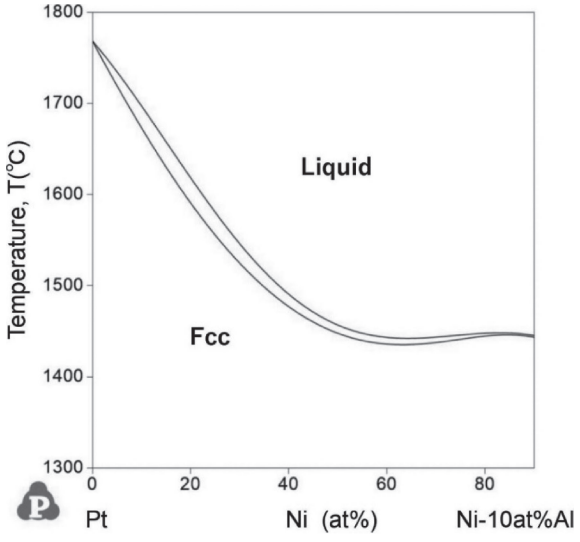

Fig. 10 Vertical section of the calculated Ni-Al-Pt ternary phase diagram. When Pt is added to Ni-10% Al alloy to increase the melting point, Pt must be added at least 50 at%.

the calculation condition, the temperature was set to be slightly higher than the liquidus of Ni-10at%Al and the time was the plateau time obtained from the heat transfer calculations, because the solute diffusion layer is mainly formed when the Ni-based alloy is in the liquid state. The specific set temperature was 1450°C, approximately 4°C

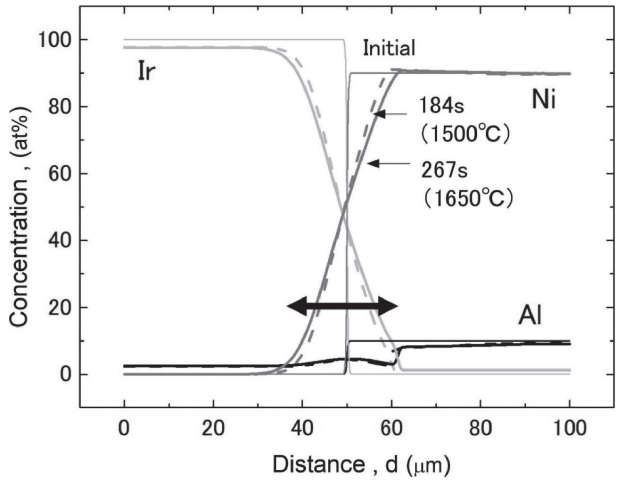

Fig. 11 Calculated diffusion profile in vicinity of Ir/Ni-10at%Al interface. The length of the diffusion region indicated by the arrow is about 25 μm which is in good agreement with experimental results.

higher than the liquidus of the Ni-10at%Al alloy (1445.4°C). This is to avoid numerical instability on the Ni-base alloy side in the diffusion couple, where the liquid/solid phase ratio fluctuates greatly due to inevitable numerical errors in diffusion calculation when the calculations were performed near the liquidus temperature.

Figure 11 shows the calculation results for the Ir sample which placed at 40 mm and molten temperature was 1650°C/1500°C, and the plateau time was 267 s/184 s, respectively. The concentration profiles of both Ni and Ir can be regarded as symmetrical with respect to the original interface set at 50 μm. The length indicated by the arrow in the figure is 25 μm. The experimental results (Fig. 8) and the calculated diffusion distance of Ir are in good agreement. The alloying element, Al does not decrease monotonically towards the Ir side, which is due to the up-hill diffusion of Al. In fact, according to the diffusion database the diagonal term of the interdiffusion coefficient, D_{AlIr} (Al diffusion caused by Ir concentration gradient), showed positive when the Ir concentration was below about 40 at% in the calculated concentration distribution at 1450°C. The concentration distribution in Fig. 8, the width of the Al concentration change is narrower than that of Ir and Ni and the change is observed on the high Ir concentration side. In Fig. 8(a), the Al concentration peak at a distance of about 22 μm is also thought to be caused by the up-hill diffusion effect of Al. The calculated Al concentration in the interdiffusion layer decreases at about 12 μm on the Ni alloy side from the initial interface. This concentration drop corresponds to the solid-liquid interface at 1450°C and results in a slight deviation from the experimental observation in which the sample is furnace-cooled to room temperature.

The result from the Re sample shows that the change in the concentration distribution is observed only on the Re side (Fig. 12), which is in good agreement with the experimental result (Fig. 9). Since the Re sample is not assumed to be a sintered body in the numerical calculation, the concentration distribution appearing only in the Re sample is not due to the Re sample being a sintered body, but it is a characteristic of the Re element. Here, the distance of concentration changes

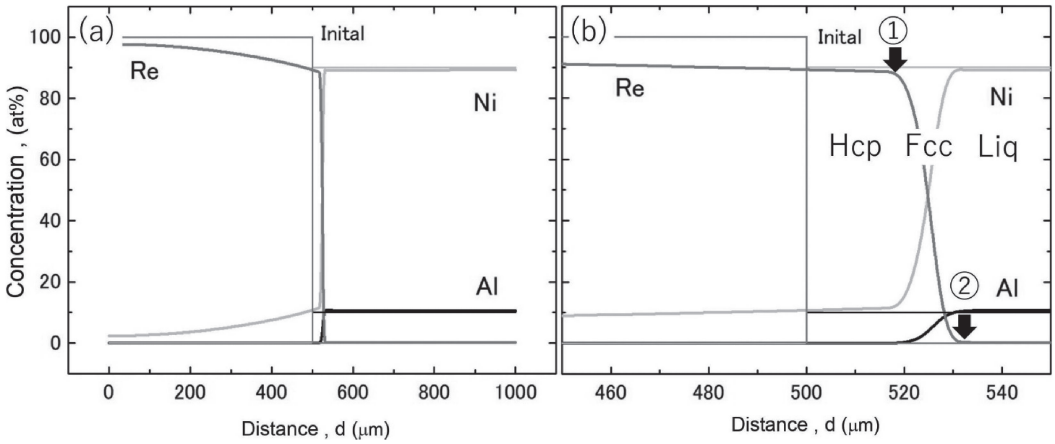

Fig. 12 Calculated diffusion profile in vicinity of Re/Ni-10at%Al interface. (a) Concentration distribution over the entire calculation area, (b) Enlarged concentration profile near the initial interface; in the case of Re, two phase boundaries, hcp/fcc and fcc/liq interfaces, are formed.

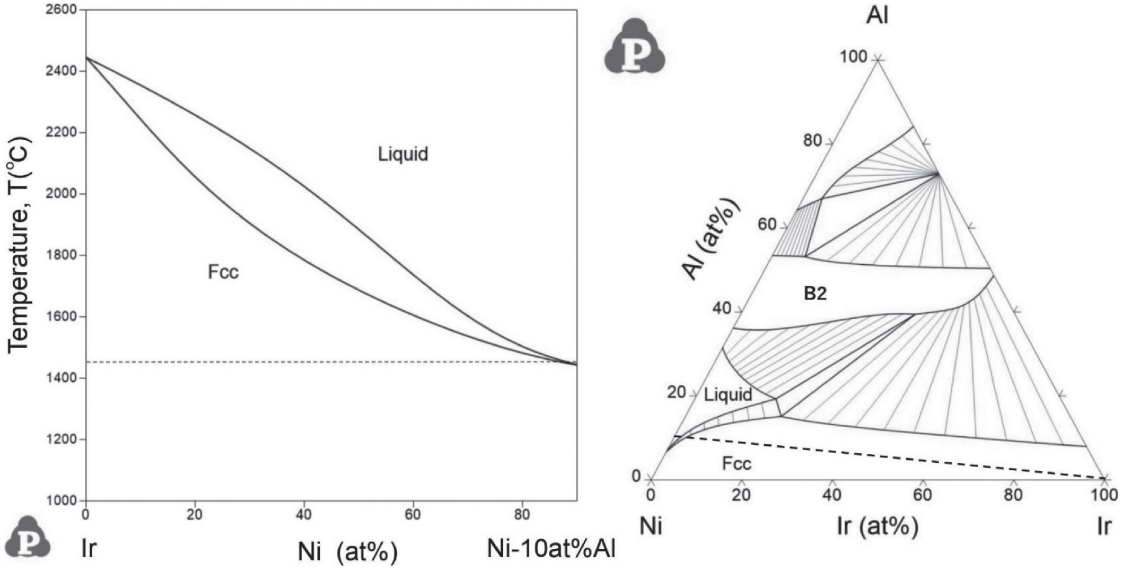

Fig. 13 Vertical and isothermal (1450°C) section of calculated Ni-Al-Ir ternary phase diagram.

on the Re side is much longer than that in the experiment. Calculation of the diffusion database shows that the diffusion coefficient of Ni in the Re-rich hcp phase is about $3 \times 10^{-10}\,m^2/s$ at 1450°C, which is about 10,000 times larger than that in Ir and Pt at the same temperature. Extrapolating the experimental diffusion coefficients of Ni-Re binary alloys[13] to 1450°C, the diffusion coefficients are almost equal to those in Ir and Pt, so the calculated diffusion distance into the Re sample is not highly reliable.

Figures 13 and 14 show the longitudinal sectional phase diagrams for pure substance X (X = Ir, Re) and Ni-10at%Al, and isothermal cross sections at 1450°C. The dotted line in the figure corresponds to the temperature of 1450°C in the longitudinal section and the concentration of Ni-10at%Al and X (X = pure Ir or Re) in the isothermal section, respectively. The phase diagram shows that no large concentration gap is formed at the solid-liquid interface between pure Ir and Ni-10at%Al alloy, and that a smooth concentration distribution is formed near the interface because the fcc phase is stable regardless of Ir concentration in the solidified state.

In the case of the Re/Ni-10at%Al system, on the other hand, the formation of a Re-enriched layer on the Ni-based alloy surface is difficult due to the characteristics of the phase diagram, as shown in Fig. 14. The longitudinal sectional phase diagram of the Re system is not a simple complete solubility type as in the Ir system. The isothermal cross section shows that the molten metal is expected to be in equilibrium with two solid phases, the hexagonally closed packed (hcp) and face-centered-cubic (fcc) structures. As shown in Fig. 12(b), near the interface between the Re sample and Ni-10at%Al, the phases are arranged in the order hcp/hcp+fcc/fcc/fcc+liquid/liquid. The concentrations at the interface positions indicated by ① and ② in the figure correspond to the phase boundary concentrations in the phase diagram. In other words, the dotted line in the longitudinal cross section (1450°C) and the isothermal cross section show that Re is not soluble in the liquid phase, i.e., on the Ni-rich side, and thus cannot form a diffusion layer, and that only Ni can diffuse into the hcp phase up to 20 at%. In the experiment, Al is distributed below 10 at% in both the Ni

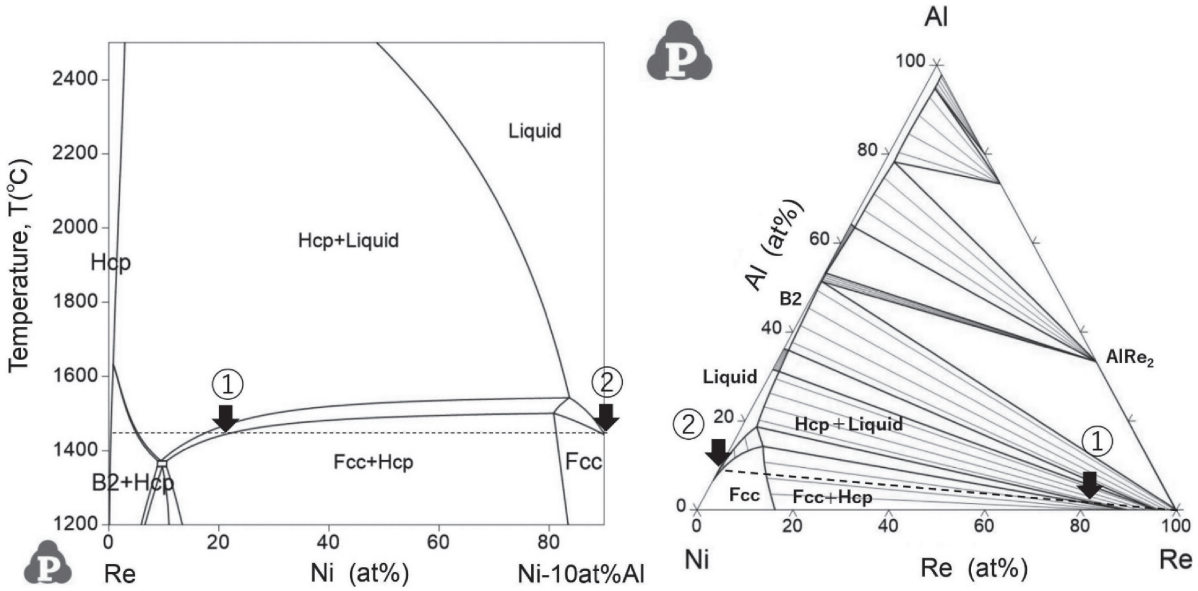

Fig. 14 Vertical and isothermal (1450°C) section of calculated Ni-Al-Re ternary phase diagram.

alloy and the Re sample. As in the case of Ir, the Al-Kα and Re-Mζ peaks are close together, making it difficult to measure dilute Al in high concentrations of Re by EDS analysis. When EDS analysis was carried on the areas, where the Ni-based alloy and Re were not diffusion bonded due to voids and cracks, Al was detected at about 10 at% in the Re sample, though Ni was not detectable. This means that it is difficult to measure the Al concentration distribution in the Re sample by EDS analysis, except in areas where Re concentration is reduced due to the interdiffusion of Ni, and Al does not appear to have diffused into the Re sample as shown in Fig. 9. Qualitatively, the concentration distribution in the Re sample shown in Fig. 9 can be explained by thermodynamic analysis using the diffusion simulation and equilibrium phase diagrams, indicating that the solute diffusion layer is only observed in the Re sample is not the result of inherent properties of the sintered microstructure. Together with the results for the Ir system, the diffusion simulation allowed for the reasonably accurate prediction of the properties of the cast-coating interface.

Finally, the applicability of cast-coating with the precious metals used in this study to Ni-based superalloy components is discussed. As shown by the results, the application of cast-coating is difficult for Pt because of liquidus depression caused by contact with Ni-based alloy. It is difficult for Re also, because it is not diffusively absorbed into the surface of Ni-based alloy. On the other hand, Ir has the strong potential for application.

In general, the unidirectional solidification process used in manufacture of turbine blades, more than one hour is required for the liquid phase to completely solidify. Therefore, calculations were carried out under the same conditions as in Fig. 11, with only the holding time at the liquidus temperature extended to one hour, to predict the extent of Ir diffusion into the molten Ni-10at%Al alloy. The result is shown in Fig. 15. According to the result, the thickness of the diffusion layer in the sample was about 200 μm. This value is considered to be sufficiently thin for Ir to localize in the Ni-based alloy and act as a surface modification layer. Therefore, it is expected that Ir elements can be cast-coated in the unidirectional solidification process even as a pure state, while the pure Pt is currently impractical but various considerations are being made based on the results of the present study.

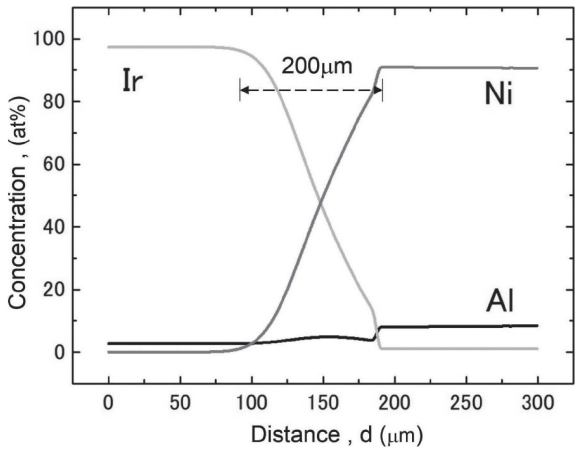

Fig. 15 Calculated diffusion profile in vicinity of Ir/Ni-10at%Al interface. The system temperature is held at the liquidus for 1 hour. The calculated diffusion length is acceptable as a surface modification formed in a cast-coating process.

4. Summary

In this study, the feasibility of a process for surface modification of Ni-based alloys simultaneously with casting by cast-coating with high melting point rare metals was investigated using a combination of casting model experiments and numerical calculations. Pt, which is already in practical use as an oxidation-resistant bond coat for Ni-based superalloys, and Re and Ir, which have particularly high melting points, were selected as candidate elements for cast-coating.

Casting model experiments:

Small specimens of Pt, Re and Ir pure materials were placed inside a mold designed for unidirectional solidification, and molten Ni-10at%Al alloy was poured into the mold to measure temperature and observe the concentration at the interface between each elemental sample and the Ni alloy. The small specimens were engulfed in solid approximately 100–300 s after casting; Pt was completely dissolved except for some parts, Ir formed an interdiffusion layer of 20–30 μm, and Re was hardly soluble in Ni alloy side.

Numerical calculations:

The sample temperature was predicted from the solidification heat transfer analysis (enthalpy method) using the temperature plateau time recorded by thermocouples installed inside the mold as an indicator. The heat transfer parameters required for the prediction were determined to minimize the error between the actual measurements and the calculations. The obtained thermal conditions were applied to the diffusion simulation, and the experimental concentration distribution at the interface between the Re and Ir specimens and the Ni-10at% alloy showed good agreement with the calculation results. This shows that diffusion simulation can accurately predict the applicability of cast-coating. Furthermore, Ir showed high potential as cast-coating even under turbine blade manufacturing conditions where the molten metal is held for long periods of time.

Acknowledgements

This work was supported by Innovative Science and Technology Initiative for Security Grant Number JPJ004596, ATLA, Japan.

REFERENCES

1) T. Okamoto and K. Nose: *The Latest Technological Trend of Rare Metals*, (CMC Publishing Co., Ltd., Tokyo, 2012) p. 170.
2) H. Nakae: *Engineering Casting*, (Sangyo Tosho Publishing Co., Ltd., Tokyo, 1995) p. 178.
3) T. Noguchi and S. Kamota: J. JFS **70** (1998) 920–927.
4) T. Watanabe: Imono **55** (1983) 381.
5) S. Aso, M. Nakanishi, S. Goto, H. Ike and Y. Shobuzawa: J. JFS **73** (2001) 155–160.
6) K. Okada, S. Goto, S. Aso and Y. Komatsu: J. JFS **74** (2002) 497–505.
7) Y. Tsunekawa: J. JFS **76** (2004) 487–493.
8) https://computherm.com/docs/thermodynamic_manual.pdf.
9) C. Zhang, J. Zhu, A. Bengtson, D. Morgan, F. Zhang, W.-S. Cao and Y.A. Chang: Acta Mater. **56** (2008) 2576–2584.
10) *Metals Handbook*, 3rd ed., (Maruzen publishing, Tokyo, 2000) p. 13.
11) K. Gunji: Tetsu-to-Hagané **80** (1994) N266–N280.
12) I. Ohnaka: *Introduction to Computer Heat Transfer and Solidification Analysis*, (Maruzen publishing, Tokyo, 2021) p. 336.
13) C. Neubauer, D. Mari and D. Dunand: Scr. Metall. Mater. **31** (1994) 99–104.